DOI: 10.1002/((please add manuscript number))
Article type: Communication

Engineering Hierarchical Architectures for Bio-Inspired Photonics

Shengyang Chen, Bastian Haehnle, Xavier van der Laan, Alexander J.C. Kuehne, Ioan Botiz, Paul N. Stavrinou, Natalie Stingelin**

S. Chen, X. van der Laan, Prof. N. Stingelin
Department of Materials and Centre of Plastic Electronics, Imperial College London, London SW7 2AZ, United Kingdom

B. Haehnle, Prof. A. J. C. Kuehne
Institute of Organic and Macromolecular Chemistry, Ulm University, Albert-Einstein-Allee 11, 89081 Ulm, Germany

Prof. A. J. C. Kuehne
DWI – Leibniz-Institute for Interactive Materials, Forckenbeckstr. 50, 52074 Aachen, Germany

Dr. I. Botiz
Interdisciplinary Research Institute on Bio-Nano-Sciences, Babes-Bolyai University, Treboniu Laurian nr. 42, Cluj-Napoca 400271, Romania

Prof. P. N. Stavrinou
Department of Engineering Science, University of Oxford, Parks Road, Oxford OX1 3PJ, United Kingdom
E-mail: paul.stavrinou@lincoln.ox.ac.uk

Prof. N. Stingelin
School of Materials Science and Engineering and School of Chemical and Biochemical Engineering, Georgia Institute of Technology, Atlanta, Georgia 30332-0245, USA
E-mail: natalie.stingelin@mse.gatech.edu

Keywords: biomimetics, hierarchical materials, self-assembly, polymer nanoparticles, photonics

Nano- and micro-engineered hierarchical structures provide excellent opportunities for mimicking optical elements and functionalities found in nature. The vivid iridescent response from particular Butterfly wings is as an excellent example of such arrangements, which typically relies on both physical structuring and pigmentary inclusions. Nevertheless attempts to replicate these sophisticated structures has proved challenging. Here we construct such hierarchical assemblies in a straight-forward manner via the use of embossed diffraction gratings and solution-based light-absorbing micro-spheres made of a conjugated polymer as pigments. A series of model systems highlight how simple geometrical relationships enable particle assembly into specific sites. These sphere-in-grating assemblies support a diverse array of patterns, spanning ordered to disordered arrangements, hexagonally or randomly packed structures with mono- and multilayer architectures. Furthermore, controlling the nucleation of the sphere assembly is shown to offer a stable cubic arrangement. The approach provides a versatile route for obtaining multifunctional assemblies, suitable for applications in biomimetics, photonics and beyond.

Many colors in nature such as those frombutterfly wings, bird plumages and fish skins

originate from more than one coloration mechanism — often a combination of structural and pigmentary coloration.[1–3] This fact makes it generally challenging to mimic such effects as architectures are required to exhibit modulation of dielectric properties in 1-, 2-, or 3-dimensions, in addition to spatially arranged wavelength-selective absorbing/emitting pigments, all in a single component. Some promising attempts have focused on bio-templating, whereby moulds are created directly from nano- and micro-structures extracted from a creature.[4,5] These delicate specimens, however, can be easily damaged especially as additional processing steps are often required to incorporate pigments; moreover, only small areas can usually be reproduced. Other approaches have considered e-beam lithography, a top-down approach, which principally allow high-resolution, precise fabrication of desired architectures, followed by an assembly of pigments, to create structural coloration[6,7]. Nevertheless, this approach can be highly time-consuming, expensive and is often limited to relatively small areas.

In this communication, we explore a straight-forward alternative that utilizes the arrangement of hierarchical sphere-in-grating structures to achieve vivid optical responses (**Figure 1**a). Such architectures rely on the combination of optical gratings (surface relief structures with one-dimensional periodicity) and micro-sized spheres of absorbing pigments, readily assembled into specific patterns, to provide coloration via light diffraction.

Atactic polystyrene (*a*-PS) was selected as the grating material since *a*-PS is known to exhibit no absorption band in the visible spectrum, and its amorphous nature minimizes optical losses resulting from undesired light scattering effects. Gratings were produced by embossing thin *a*-PS films with an elastomeric stamp,[8–10] resulting in samples that appear to the eye as a relatively homogenous purple color (**Figure 1**b). The quality of the gratings was quantitatively assessed by recording their optical diffraction pattern; an example of which is displayed in Figure S1 (Supporting Information). The highly symmetric diffraction profile and the clean, sharp diffraction orders suggest excellent overall homogeneity of the PS gratings.

To proceed we turn to selecting the pigment: highly monodisperse micro-spheres of the conjugated copolymer poly(9,9-dioctylfluorene-alt-divinylbenzene) (F8DVB) are accessible via dispersion polymerization, and were chosen due to their optical absorption (centered around 380 – 400 nm) and well-defined emission around 510 nm (see Figure S2).[11,12] Hierarchical assemblies were then created by incorporating F8DVB spheres into the *a*-PS gratings via a soft-blade coating process, illustrated in **Figure 1**a. Following the deposition of the F8DVB spheres a notable color change was immediately apparent: the purple response from the unfilled state is now visually a metallic-like yellow/golden color upon filling with the F8DVB spheres (**Figure 1**b). The striking change highlights the coupled effect of the pigments *and* the grating structure.

Further examinations sought to scrutinize the hierarchical architectures on different length scales, in particular, the extent of filling, sphere assembly and, generally the overall homogeneity. We started with scanning electron micrographs (SEM), which allowed us to obtain information of the assembled structures within three adjacent grooves. We found the F8DVB spheres assembled in a highly ordered, hexagonally close-packed arrangement (**Figure 1**b) and that this arrangement was maintained with excellent sphere filling over a 50 μm x 50 μm region, as the fluorescence micrograph in **Figure 1**c demonstrate. For this later experiment, the F8DVB spheres were excited at 380 nm (the absorption maximum, cf. Figure S2) and allowed us to track the emission between 500 nm and 550 nm. Note it is only the emission from the fluorescent F8DVB sphere arrays that is observed as the polystyrene gratings do not emit.

To further quantify the overall arrangement of the sphere-in-gratings assemblies, we recorded a diffraction pattern, captured over a 1-mm diameter laser spot (see Supporting Information for details); an typical pattern is shown in the inset of **Figure 1c**. The resulting symmetric, sharp and intense features provide a strong indication for the uniformity that can

be achieved over a large area for this hexagonal-packing motif. A view further supported by the excellent agreement with a Fast-Fourier Transform technique used to simulate diffraction patterns of sphere-in-grating structures (see Figure S3). Note the excellent filling of F8DVB spheres was also evident from other techniques discussed in the Supporting Information and presented in Figure S4. We also draw attention to results using fluorescent magnetic polystyrene spheres, which were similar in size to the F8DVB spheres and also assembled into a hexagonal-packing motif. The resulting image is shown in **Figure 1**d and highlights the versatility of the method, using spheres with different functionality.

An interesting question is whether other controlled sphere assemblies, beyond hexagonal motifs, may be obtained? To this end, we fabricated hierarchical sphere-in-grating architectures where the grating dimensions and sphere size — the groove width, *a*, and the sphere diameter, *D* — were varied according to *D/a*. This was achieved through the choice of sphere type (PS *vs*. silica) and the master embossing grating. SEM micrographs in **Figure 2** show the numerous sphere-in-grating assemblies that were produced (**Figure 2**; the *D/a* values are linked to the corresponding SEM micrographs by the dashed and dotted lines). The bars on the left of the diagram display the *D/a* values for hexagonal- and cubic packing (D_h/a and D_c/a, respectively) as obtained from the following, simple geometrical relationships:

$$\frac{D_h}{a} = \frac{2}{2 + \sqrt{3}(\mathrm{n} - 1)} \tag{1}$$

$$\frac{D_c}{a} = \frac{1}{\mathrm{n}} \tag{2}$$

where n is an integer that refers to the number of spheres along one of the close packed directions (see Supporting Information and Figure S5 for details).

A wide variety of sphere assemblies are realised depending on the ratio, *D/a*. For *D/a* values close to 1, a linear 1D-array of spheres along the grooves is formed, whereas a zig-zag

sphere arrangement results when *D/a* takes values less than 1. Further decreasing the ratio *D/a* now approaches the range where either hexagonal packing or cubic packing becomes geometrically favorable and the resulting assembly becomes highly sensitive to the *D/a* ratio. Hexagonal packing was observed at *D/a* values of 0.52, 0.37, and 0.30 for n = 2, 3 and 4 respectively. These values are close to the optimal values required for hexagonal packing with D_h/a = 0.54, 0.37, and 0.28 for the same n values, indicated on the left-side of **Figure 2** by the shaded bars. Notably, when *D/a* values were close to the optimal values for cubic packing, *i.e.* D_c/a = 0.50 and 0.33 for n = 2 and 3, clusters of cubic-packed arrangements were found in a only a few areas; as the examples in **Figure 2** for *D/a* for 0.48 and 0.31 illustrate. Indeed the samples appeared to be dominated by random packing and long-range ordered cubic packing was rarely observed.

The challenge to realize cubic motifs, and more generally the differences between hexagonal *vs* cubic assembly, may be linked to their respective packing densities. Maximum hexagonal packing density requires $D/a = 0.74$ whereas for a cubic assembly, the value is closer to 0.52. We propose that as the packing density of randomly assembled spheres can reach as high as 0.64,[13] random packing will likely dominate over cubic packing and to a lesser extent with hexagonal packing. ~~Another factor is the increased challenge of aligning two spheres perfectly perpendicular to the groove direction.~~

Intriguingly, an complex assembly of superstructures can also be observed. An example is shown in **Figure 2** for the *D/a* combination of 0.24 – which is close to the 0.22 optimal value for hexagonal packing (n = 5). In this rather specific case, regular zig-zag defects *within* the hexagonal lattices locally form. However, in common with most $D/a \approx 0.22$ scenarios the repetition of a single motif over multiple periods was not found, rather the attendant decrease in long-range order was presumably due to the variety of packing motifs that become possible (see Figure S6–8, Supporting Information). This situation became more pronounced as *D/a* values

were decreased less than 0.22 and under such conditions, only random-packing configurations were obtained.

While SEM sufficiently probes relatively small length scales of the assemblies, to provide greater insight over larger-scales, and assess the utility of the above *D/a* relationships, we turned to optical diffractometry. For this technique, regular well-packed arrangements can be expected to offer bright routine diffraction patterns, whereas randomly packed spheres will tend to act as diffusers due to the structural disorder of the assembly.

Angle-resolved transmission spectra were recorded as the structures were rotated, in a plane perpendicular to the incident light, to provide 0°- (grey), 60°- (red) and 90°- (green) sampled directions with respect to the original (0° alignment). For samples with geometries close to optimal D_h/a values, the 2D diffraction patterns are displayed in **Figure 3**: from top to bottom, D/a = 0.52 (row 1) and 0.48 (row 2), compared to the optimal D_h/a = 0.54 for n = 2; D/a = 0.37 (row 3) and 0.36 (row 4) (optimal D_h/a = 0.37, n = 3); and D/a = 0.30 (row 5) and 0.31 (row 6) (optimal D_h/a = 0.28, n = 4). Accompanying electron micrographs are also shown in the left-hand panel to illustrate the sphere-in-grating packing.

For hexagonally packed samples (**Figure 3**, rows 1 and 3 for n = 2 and 3), we observe symmetric, sharp and intense diffraction orders, as expected for well-ordered structures. The clear diffraction patterns, particularly for the 60° and 90° cases, arise from well-ordered regions that dominate over any scattering effects that would result from a disordered arrangement; the spectra highlight the long-range order that is present for assemblies under these *D/a* scenarios. The quality of these results may be further appreciated by comparing spectra, obtained under similar conditions, for the other scenarios of **Figure 3**. Here only weak diffraction spectra are observed, and for these cases, the SEM reveal a random sphere packing, see e.g. **Figure 3**, rows 2 and 4.

In addition to the *D/a* ratio, we can expect other parameters to be involved in the sphere-in-grating assembly. For example, deciding on the number of spheres vertically positioned within the grooves was also found to play an important role, as the insets in **Figure 3** (left panel) illustrate. An appropriate choice of sphere size to groove depth allow for a single layer of deposited spheres within the grooves (**Figure 3**, rows 1 and 2) while choosing smaller spheres leads to growth of multiple layers (**Figure 3**, rows 3 to 6). As in the earlier studies, whether the spheres form mono- and bilayer-like architectures within the grating grooves (**Figure 3**, rows 1 to 4), ordered and disordered assemblies may be clearly distinguished via their diffraction patterns. This is especially true with regard to the sharpness and intensities of the diffraction points, as shown in Figure 3 insets in columns 2 to 4. In the case of trilayers (**Figure 3**, rows 5 and 6), the presence of increased disorder results in spectral peak broadening of the diffraction profiles (0º cuts). Overall it is clear that hexagonally packed samples led to sharper peaks for most diffraction orders compared to those found for randomly packed assemblies (see Figure S9). This observation supports the view that in hexagonally packed samples, there are fewer defects that would result in scattering compared to randomly packed samples.

Some fascinating observations emerge with multilayer sphere-assemblies within the gratings, particular when referencing the layers in the context of localized defects, **Figure 4**. Spheres in the top layer, for instance, can be found at a position where two spheres in the layer below touch (**Figure 4**a) and lead to a coordination number of 10 (i.e. ten spheres surrounding a single one). This strongly contrasts the situation for example in natural opals, where spheres in adjacent layers nestle on top of tetrahedral sites,[14] which leads to hexagonally close-packed (hcp) or face-centered cubic (fcc) colloidal crystal structures with a coordination number of 12 (**Figure 4**b). This difference between certain spheresin-grating structures and natural opals underlines the importance of the 'confinement' effect the grating structure/grating walls have on the assembly. Of course, the proximity of groove walls can also have a negative influence,

e.g., through heterogeneous nucleation, leading to sphere disorder, especially when *D/a* becomes small (< 0.22).

Nucleation generally plays a significant role in determining packing nature. Thereby it is important to note that nucleation of sphere assembly can start both from the groove walls where spheres impinge and further movement is restricted, as well as from other sites such as the middle of the grooves, as indicated in the micrograph of **Figure 4**c (left panel). In either case, grains can result with various orientations. In other words, a current polycrystalline layer can in turn template further sphere assembly on the layer above, the result being an increase in the degree of disorder through forming an increasing number of grains in the subsequent layers; a process that will eventually lead to amorphous solids, *i.e.*, randomly packed systems.

Sphere nucleation can also be beneficial and manipulated by using different grating geometries. In a preliminary demonstration, we focused on V-shaped gratings with an apex angle of 73.2º. Under such geometrical conditions, spheres originate from the bottom of the grooves to form nearly perfect fcc lattices with the (111) planes parallel to the groove sidewalls[15] (**Figure 4**c, right panel). An observation that highlights how the manipulation of sphere nucleation can render cubic sphere packing stable.

To conclude, hierarchical sphere-in-grating architectures were successfully fabricated and shown to display an optical response, not unlike those found in nature, *e.g.*, in butterfly wings. The structures themselves demonstrate how powerful the effect of combining structural coloration effects with a pigmentary mechanism can be. Our findings provide some understanding of how spheres may assemble into mono- and multilayer-like assemblies in the grating structures, with both ordered hexagonal and cubic structures reliably produced. Key parameters are identified, namely the selection of *D/a* and groove shape from which desired structures/motifs may be engineered. In addition, our simple *D/a*-assembly relationship can predict scenarios where complex superstructures, observed previously,[16,17] are assembled.

Importantly, the guidelines established here assist in creating, if desired, fully disordered assemblies of pigments which have been difficult and time-consuming to produce synthetically.[17–19] Such architectures should prove interesting in certain photonics applications and may be exploited in, for example, random lasing structures.[20,21] Clearly, further use of hierarchical sphere-in-grating structures is not limited to the materials studied here and any number of contemporary functional materials, such as metallic nanoparticles, core-shell QDs, magnetic spheres (**Figure 1**d) or ferroelectric gratings (see Figure S10, Supporting Information) can be equally adapted in a variety of sphere-in-grating assemblies. The great strength of our approach lies with the use, and the relative simplicity, of the fabrication process that exploits commonly used embossing procedures and straight-forward coating methodologies.

Supporting Information

Supporting Information is available from the Wiley Online Library or from the author.

Acknowledgements

We acknowledge support from the EPSRC: EP/K03099X/1 – Centre for Innovative Manufacturing in Large Area Electronics, for financial support. S. Chen acknowledges the fellowship sponsored by the China Scholarship Council. N. Stingelin and I. Botiz acknowledge the Marie Skłodowska-Curie Actions Innovative Training Networks "H2020-MSCA-ITN-2014 INFORM-675867" for funding.

Received: ((will be filled in by the editorial staff))
Revised: ((will be filled in by the editorial staff))
Published online: ((will be filled in by the editorial staff))

References

[1] A. L. Ingram, A. R. Parker, *Philos. Trans. R. Soc. Lond. B. Biol. Sci.* **2008**, *363*, 2465.

[2] B. D. Wilts, A. Matsushita, K. Arikawa, D. G. Stavenga, *J. R. Soc. Interface* **2015**, *12*, 20150717.

[3] A. C. Price, C. J. Weadick, J. Shim, F. H. Rodd, *Zebrafish* **2008**, *5*, 297.

[4] R. E. Rodríguez, S. P. Agarwal, S. An, E. Kazyak, D. Das, W. Shang, R. Skye, T. Deng, N. P. Dasgupta, *ACS Appl. Mater. Interfaces* **2018**, *10*, 4614.

[5] F. Liu, Y. Liu, L. Huang, X. Hu, B. Dong, W. Shi, Y. Xie, X. Ye, *Opt. Commun.* **2011**, *284*, 2376.

[6] M. Burresi, L. Cortese, L. Pattelli, M. Kolle, P. Vukusic, D. S. Wiersma, U. Steiner, S. Vignolini, *Sci. Rep.* **2014**, *4*, DOI 10.1038/srep06075.

[7] S. Zhang, Y. Chen, *Sci. Rep.* **2015**, *5*, 16637.

[8] N. Stutzmann, T. A. Tervoort, C. W. M. Bastiaansen, K. Feldman, P. Smith, *Adv. Mater.* **2000**, *12*, 557.

[9] G. Fichet, N. Stutzmann, B. V. O. Muir, W. T. S. Huck, *Adv. Mater.* **2002**, *14*, 47.

[10] Y. Xia, G. M. Whitesides, *Angew. Chemie Int. Ed.* **1998**, *37*, 550.

[11] S. Ciftci, A. J. C. Kuehne, *Macromolecules* **2015**, *48*, 8389.

[12] A. Mikosch, S. Ciftci, A. J. C. Kuehne, *ACS Nano* **2016**, *10*, 10195.

[13] A. Donev, I. Cisse, D. Sachs, E. A. Variano, F. H. Stillinger, R. Connelly, S. Torquato, P. M. Chaikin, *Science* **2004**, *303*, 990.

[14] J. V. Sanders, *Nature* **1964**, *204*, 1151.

[15] X. V Li, R. M. Cole, C. A. Milhano, P. N. Bartlett, B. F. Soares, J. J. Baumberg, C. H. De Groot, *Nanotechnology* **2009**, *20*.

[16] L. Malaquin, T. Kraus, H. Schmid, E. Delamarche, H. Wolf, *Langmuir* **2007**, *23*, 11513.

[17] Y. Xia, Y. Yin, Y. Lu, J. McLellan, *Adv. Funct. Mater.* **2003**, *13*, 907.

[18] S. M. Yang, G. A. Ozin, *Chem. Commun.* **2000**, 2507.

[19] P. D. García, R. Sapienza, Á. Blanco, C. López, *Adv. Mater.* **2007**, *19*, 2597.

[20] S. Gottardo, R. Sapienza, P. D. García, A. Blanco, D. S. Wiersma, C. López, *Nat. Photonics* **2008**, *2*, 429.

[21] N. M. Lawandy, *Nat. Phys.* **2010**, *6*, 246.

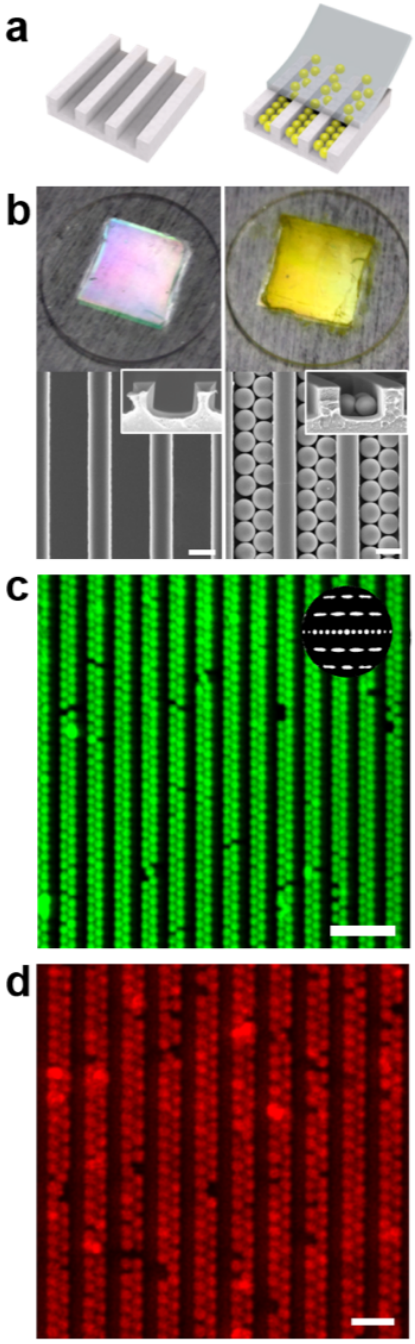

Figure 1. Mimicking the color effects in butterfly wings via hierarchical architectures comprising spheres of the F8DVB (as pigment) and polystyrene (PS) diffraction gratings. (a) Convective self-assembly process of F8DVB spheres onto surface relief structures by soft-blade coating. (b) PS gratings exhibited a purple color due to light diffraction while a gold color was observed when F8DVB spheres were introduced into the gratings. The SEM micrographs of F8DVB-spheres-in-PS-grating structures revealed densely-filled, hexagonally packed F8DVB spheres. Scale bars: 2 μm. (c) Fluorescence imaging demonstrates the large-area ordering of F8DVB spheres. An excitation wavelength of 380 nm was used. Light emission was detected from 500 to 550 nm. Scale bar: 10 μm. The inset shows a 2D optical diffraction pattern of F8DVB-spheres-in-PS-grating structures. (d) Magnetic polystyrene particles assembled into PS gratings. These spheres were fluorescent when excited at 600 nm. Their emission was detected at red wavelengths employing a fluorescence microscope. Scale bar: 5 μm.

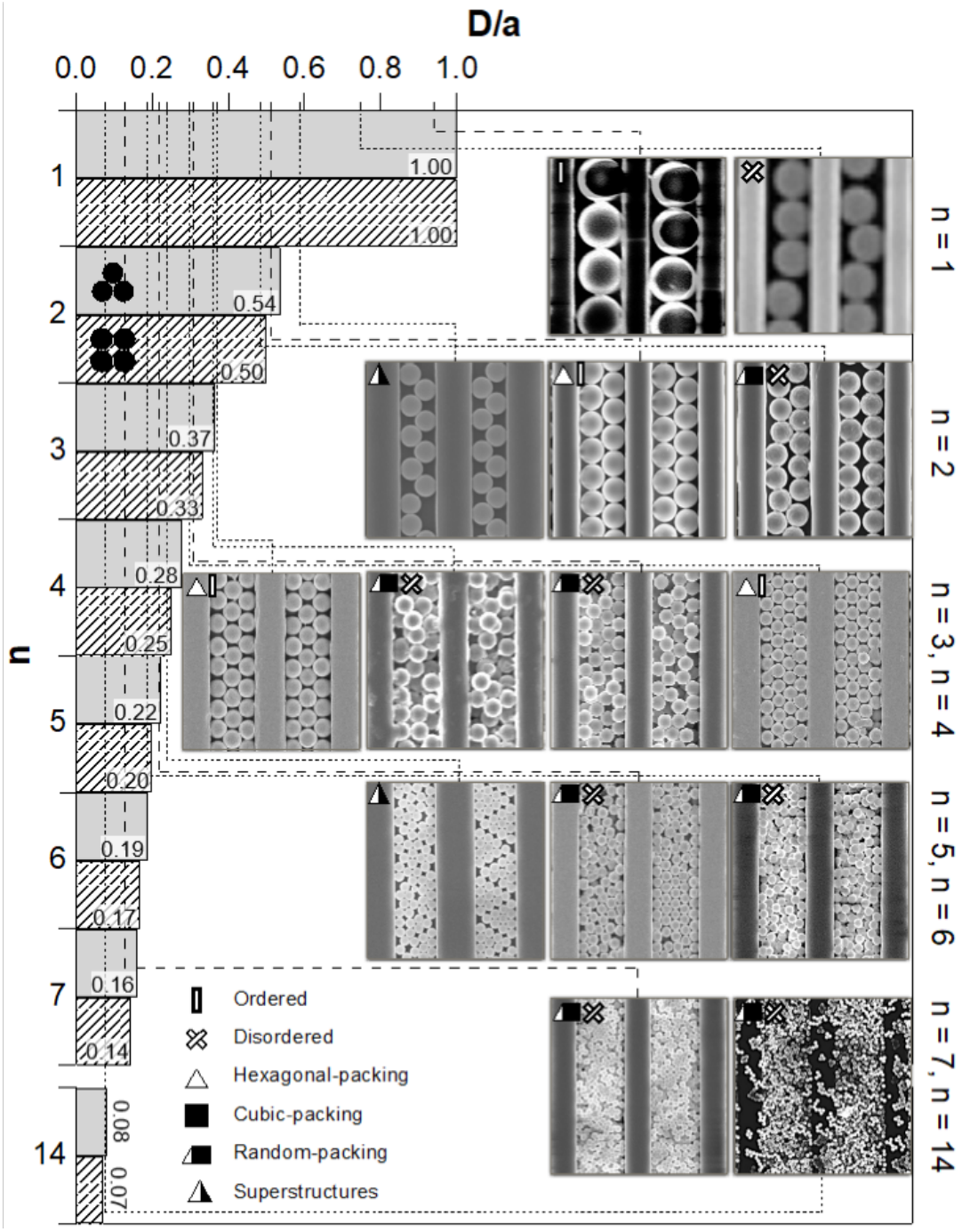

Figure 2. Geometrical relationship diagram between sphere diameter, *D*, and groove width, *a*. Here, *D/a* combinations of decreasing value were investigated. The optimal values of hexagonal-closed packing and cubic-closed packing are given by the shaded boxes on the left as comparison. n is an integer and refers to the number of spheres along one of the close packed directions. *D/a* ratios from left to right, top to bottom: 0.95, 0.74, 0.58, 0.48, 0.37, 0.36, 0.31, 0.30, 0.24, 0.22, 0.18 and 0.07.

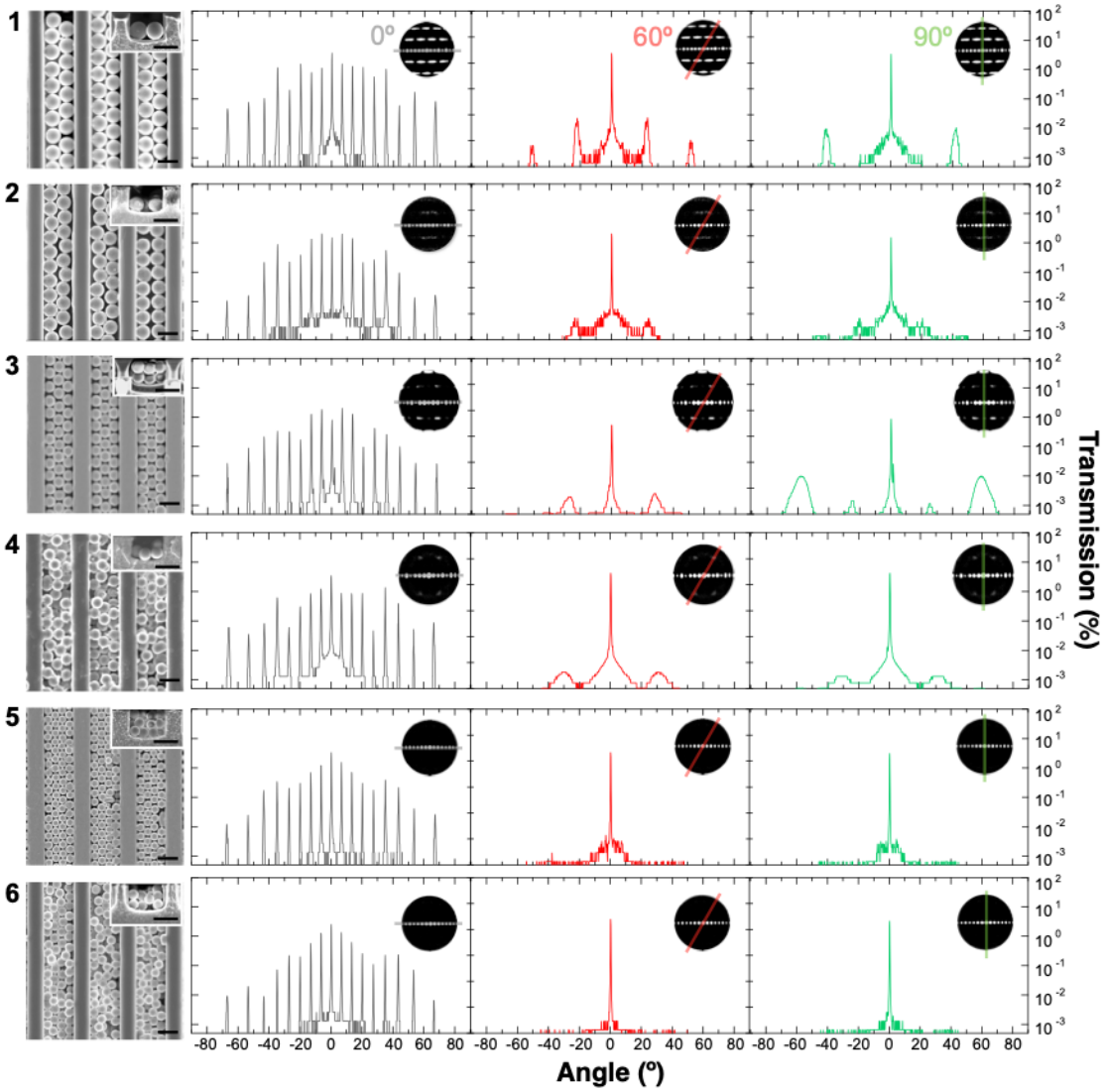

Figure 3. Degree of order in hierarchical spheres-in-grating architectures, probed by SEM (left panel, scale bar: 2 μm) and optical diffractometry. Diffraction transmission profiles along 0º (grey), 60º (red) and 90º (green) cuts are shown with 2D diffraction patterns displayed in the insets, providing quantifiable features associated with order (disorder) in monolayers, bilayers and trilayer architectures. The *D/a* ratios from top to bottom are 0.52, 0.48, 0.37, 0.36, 0.30 and 0.31.

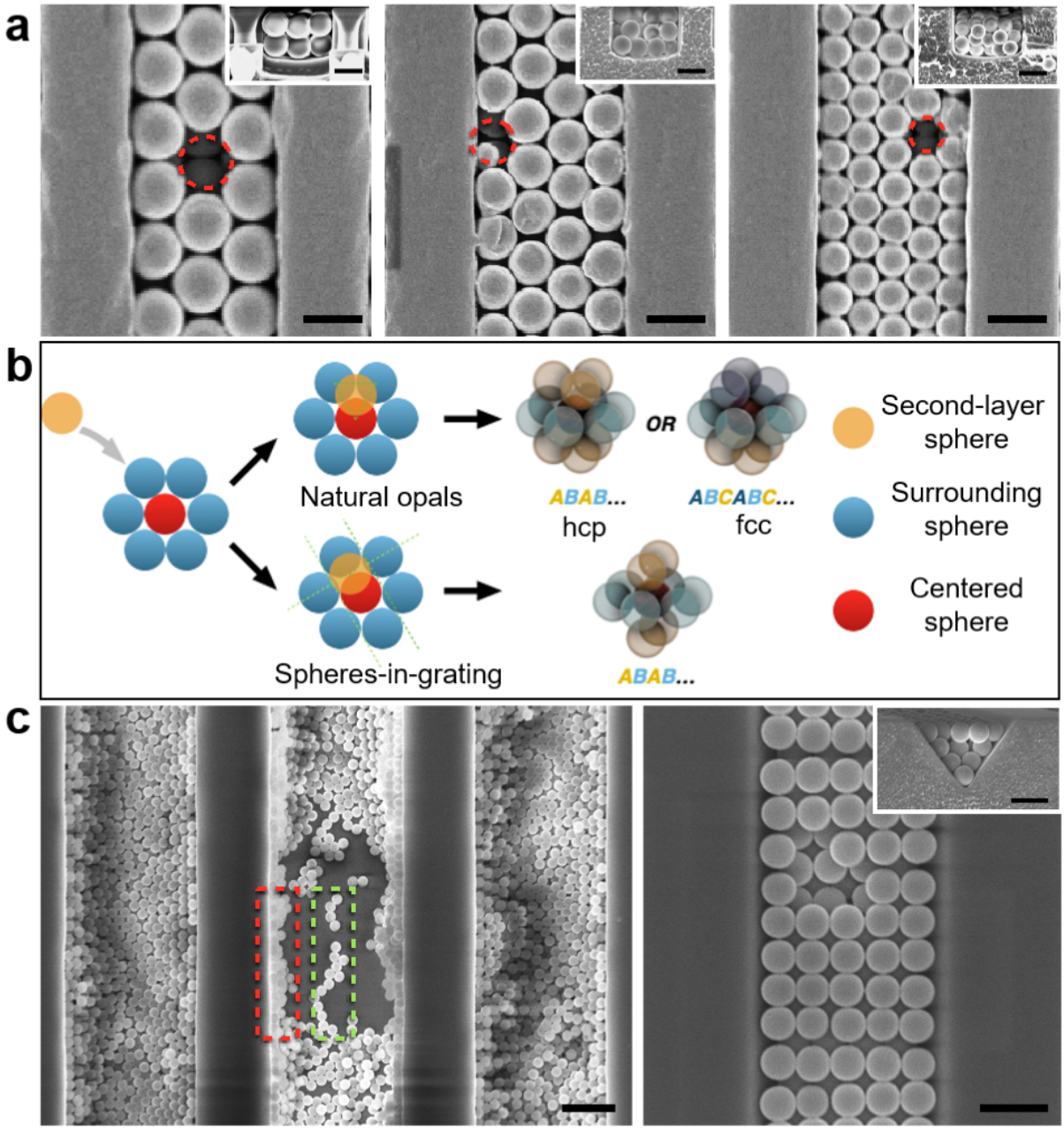

Figure 4. Influence of groove wall-nucleation on sphere coordination number. (a) A colloidal crystal structure with a coordination number of 10 is found in spheres-in-grating architectures, as observed through vacancy sites by electron micrographs. (b) The colloidal crystal structure formed is in contrast to dense hcp and fcc structures (coordination number: 12) such as those found in natural opals. (c) Electron micrographs illustrating possible nucleation sites in spheres-in-grating assemblies when D/a value is small (< 0.22). In addition to nucleation from groove walls (highlighted with the red dashed box), nucleation in the middle of the groove (highlighted with the green dashed box) can occur. The use of V-shaped gratings can enable the self-assembly of spheres from the bottom of the grooves. With an apex angle of 73.2º, cubic structures were constructed. All scale bars are 1 μm.

ToC figure: